The Equatorial Small-Angle Scattering during the Straining of Poly(ether ester) and Its Analysis

N. STRIBECK

Universität Hamburg, Institut TMC, Bundesstr. 45, 20146 Hamburg, Germany

Received 8 May 1998; revised 28 September 1998; accepted 18 November 1998

ABSTRACT: A method for the quantitative analysis of two-dimensional (2D) small-angle X-ray scattering (SAXS) patterns with fiber symmetry by successive information filtering is proposed and applied to a series of images recorded during a straining experiment of a two-phase polymer sample at a synchrotron beamline. The studied equatorial scattering is similar to the frequently discussed void scattering, but originates from an ensemble of rodlike soft domains (needles) in the sample, orientated in the direction of strain. The intensity is extracted and projected onto the equatorial plane, the ideal two-phase structure is extracted, and the 2D chord distribution is computed. This curve describes a 2D two-phase morphology made from needle cross-sections embedded in matrix material. Because interparticular correlation is found to be weak in the chord distribution, pure particle scattering is assumed. Modeling the needle cross-sections by circular disks leads to a simple theory, which allows the deconvolution of a disk diameter distribution from the chord distribution. It is shown how parameters of the disk diameter distribution can be computed without deconvolution. For the selected poly(ether ester) thermoplastic elastomer the study of the soft domain needles indicates strain-induced hardening. While for low elongation ϵ the soft needles are more compressible than the microfibrillar matrix, saturation is observed for $\epsilon > 2.5$. © 1999 John Wiley & Sons, Inc. J Polym Sci B: Polym Phys 37: 975–981, 1999

Keywords: equatorial small-angle X-ray scattering; domain diameter distribution; drawing; thermoplastic elastomers; poly(ether ester)

INTRODUCTION

Two-phase polymers with preferred orientation frequently exhibit small-angle X-ray scattering (SAXS) patterns with fiber symmetry, which can be recorded at a synchrotron beam line with high accuracy. Quite often one observes patterns with many reflections, which vary considerably as a function of tunable parameters.[1–4] After a qualitative description of the observations and a semiquantitative analysis of reflection positions as a function of the parameter values, a quantitative analysis of the image series should afford profound insight into structure. The objective of the present study is the extraction of the diameter distribution describing an ensemble of oriented rod-like domains in strained material, similar to the notion of a "hard disk fluid," developed by Cohen and Thomas.[5] In contrast to this study and an article of Porod,[6] here the data are interpreted in real space and interparticular correlation is neglected.

At first sight the analysis of a two-dimensional (2D) pattern appears to be cumbersome because of the wealth of data. But for a 2D image there do exist several methods to filter out specific information. Curves gained by such a procedure only reflect certain aspects of the morphology, and thus hopefully can be described by a simple structural model.

The first steps towards this goal have been undertaken by Bonart.[1] Based upon the mathematical relation between structure and scattering, he has proposed the analysis of projections,

Journal of Polymer Science: Part B: Polymer Physics, Vol. 37, 975–981 (1999)
 CCC 0887-6266/99/100975-07

which can be extracted from the scattering patterns and reflect a longitudinal and a transverse structure, respectively. The present study deals with projections onto the equatorial plane only (transverse structure). Following a concept of Ruland[7,8] the resulting curves are not fitted by a complex model, but analyzed step by step in order to "peel off" information. Finally, a chord distribution[9–11] is computed. Only now, based upon the observed properties of the chord distribution, an adapted model is chosen. Because this model is simple, the structural parameters can be computed directly from the chord distribution without the need to fit the data. The proposed method may especially be useful in cases where the lateral extension of domains is expected to be correlated with material properties, as in the case of semicrystalline fibers, thermoplastic elastomers, or smectic liquid crystalline polymers.

Several other authors are presently working in the field of fiber pattern analysis. The group of Wilke proposes a paracrystalline macrolattice model and fits selected cuts of the pattern simultaneously to the model.[12–14] Asherov et al.[15] model the scattering pattern based on an ideal paracrystalline model. Murthy et al.[16,17] propose the choice of model functions in elliptical cylindrical coordinates to extract features from the pattern. Thus, in addition to the longitudinal and transverse structure, they determine the orientation distribution of the scattering entities.

THEORETICAL

Definitions

Let $I(\vec{s})/V$ be the measurable SAXS intensity, normalized with respect to the irradiated volume, V. Let the magnitude of the scattering vector be defined by $|\vec{s}| = (2/\lambda)\sin\theta$, with λ being the wavelength of radiation, and 2θ the scattering angle. For the ease of notation and because treatment of absolute intensities is not intended here, let us write $I(\vec{s})$ for the normalized intensity.

In the case of a scattering pattern with fiber symmetry, it is convenient to write $I(\vec{s}) = I(s_{12}, s_3)$ in cylindrical coordinates, with $s_{12} = \sqrt{s_1^2 + s_2^2}$ and the component s_3 defining the symmetry axis of the pattern. If in the case of fiber symmetry, the tangent plane approximation is assumed to be valid; the complete information of SAXS is in a two-dimensional (2D) pattern, which can be recorded using a 2D detector.

Pattern Filtering: Equatorial Scattering

Such 2D patterns may exhibit many reflections, which may vary considerably as a function of tunable parameters. If the pattern reveals equatorial scattering, the equatorial streak may be extracted from the pattern and analyzed separately. In certain cases (if the streak is clearly separated from other reflections and does not "fan out"[18]) it should suffice to mask the measured pattern

$$I_n(s_{12}, s_3) = I(s_{12}, s_3)Y_b(s_3) \tag{1}$$

to extract a "needle scattering," $I_n(s_{12}, s_3)$, in particular, if this pattern shall only be interpreted after projecting it. $Y_b(s_3)$ is a shape function, which gives a value of 1 for $|s_3| < b/2$ and vanishes elsewhere. Thus, b is the height of the equatorial band.

In addition to the study of the needle scattering, it may be interesting to study its complement,

$$I_{\bar{n}}(s_{12}, s_3) = I(s_{12}, s_3)\ (1 - Y_b(s_3)), \tag{2}$$

if distinct reflections are observed in the direction of strain. Thus, the cross-sections of microfibrils and layer stacks can be studied as well.

When dealing with the equatorial streak of a fiber pattern, it appears suitable to extract what Bonart called "Querstruktur" (transverse structure)[1] by computing the projection

$$\{I\}_2(s_{12}) = 2\int_0^\infty I_n(s_{12}, s_3)\ ds_3. \tag{3}$$

$\{I\}_2(s_{12})$ is defined in the s_{12}-plane normal to the fiber axis. Through Fourier transformation relation it is linked to a two-dimensional two-phase system made from needle cross-sections in a matrix, as indicated in Figure 1. More precisely,

$$\mathcal{F}^2(\{I\}_2(s_{12})) = Q\lceil\gamma\rfloor_2(x_{12}), \tag{4}$$

the 2D Fourier transformation, $\mathcal{F}^2()$, of the projected intensity is the product from the invariant Q, and the 2D section of the correlation function γ in the equatorial plane. The intention of this work is the analysis of the 2D chord distribution, $g_2(x_{12})$,

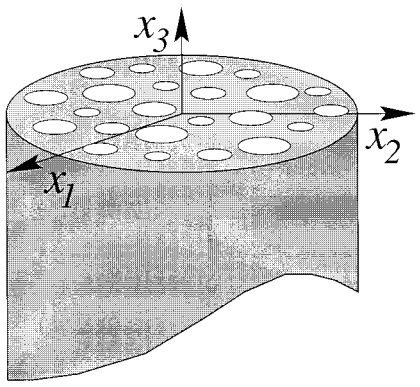

Figure 1. Sketch of the two-dimensional fiber cross-section structure, whose chord distribution is related to the projection according to eq. (3).

$$g_2(x_{12}) = f\frac{d^2\lceil\gamma\rceil_2(x_{12})}{dx_{12}^2}, \tag{5}$$

which is proportional to the second derivative of $\lceil\gamma\rceil_2(x_{12})$.

Porod's Law and Systematic Deviations

$\{I\}_2(s_{12})$ is generated by a projection process identical to that carried out by a Kratky camera. In particular $\{I\}_2(s_{12})$ exhibits Porod's law with the scattering falling off with s_{12}^{-3}. Small deviations from the predicted falloff are accounted to the nonideal structure of the real two-phase system[7,19] and corrected accordingly, leading to the 2D interference function $G_2(s_{12})$ of an ideal two-phase system

$$G_2(s_{12}) = (\{I\}_2(s_{12}) - I_{Fl})s_{12}^3/ \times \exp\left(-\frac{4}{9}\pi^2 w_t^2 s_{12}^2\right) - A_{P_2}. \tag{6}$$

A_{P_2}, Porod's asymptote of the projected SAXS intensity, is the constant governing Porod's law. The nonideal structure of the real two-phase system is described by I_{Fl} and w_t. Fluctuations of the electron density are considered by I_{Fl}, the density fluctuation background, which from practical reason is assumed to be a constant. w_t is the width of the transition zone at the domain boundary, in which the density changes smoothly. A detailed description of the procedure established to determine the interference function has been described elsewhere.[19]

Chord Distribution Analysis

General

Using eqs. (4), (5), (6), and a chosen normalization $\int_0^\infty g_2(x_{12})\,dx_{12} = A_{P_2}$, one finds that the 2D chord distribution[11,20,21] $g_2(x_{12})$ is computed from $G_2(s_{12})$ by

$$g_2(x_{12}) = \pi \int_0^\infty (\mathrm{J}_0(2\pi x_{12}s_{12}) - \mathrm{J}_2(2\pi x_{12}s_{12}))G_2(s_{12})\,ds_{12}. \tag{7}$$

Here J_0 and J_2 indicate Bessel functions of the first kind. In general, $g_2(x_{12})$ shows the distribution of chords from needle and matrix cross-sections and their correlations in the plane normal to the fiber direction.

No Correlations

In particular, if $g_2(x_{12})$ is positive everywhere, the correlations among the "disks in the plane" are negligible and $g_2(x_{12})$ represents the chord distribution of an ensemble of uncorrelated disks in the (x_1, x_2)-plane (cf. Fig. 1).

Simplification by Circles

Let the cross-section of every needle be modeled by a circular disk, then the properties of a needle diameter distribution, $h_D(D)$, are of physical interest. In the absence of correlations among the disk positions the observed chord distribution, $g_2(x_{12})$, can be written in terms of $h_D(D)$ and the intrinsic chord distribution $g_c(x_{12})$ of a disk with unit diameter. Then

$$g_2(x_{12}) = \int_0^\infty h_D(D)g_c\left(\frac{x_{12}}{D}\right)\frac{dD}{D} \tag{8}$$

is simply the superposition of compressed and expanded images from g_c weighted by the value of the diameter distribution, $h_D(D)$, which shall be studied. Equation (8) is the definition of the Mellin convolution.[8,22]

Chord Distribution of a Circle

The chord distribution of a disk with unit diameter can be computed following a proposal by Porod,[10] and has been carried out by Schmidt.[11] The result is

$$g_c(x) = \frac{x}{\sqrt{1-x^2}}, \text{ for } 0 < x < 1. \quad (9)$$

For the reason of convenient arithmetics and numerical inversion of eq. (8), $g_c(x)$ is chosen to satisfy the condition $\int_0^1 g_c(x)\,dx = 1$.

Numerical Inversion

$h_D(D)$ can be computed by numerical inversion of eq. (8) utilizing an iterative van Cittert algorithm similar to that proposed for the conventional deconvolution by Glatter.[23] The algorithm is found to converge as long as $g_2(x_{12})$ is positive everywhere. Thus, the needle diameter distribution can be computed from a measured 2D chord distribution.

Moments of a Distribution

Generally, parameters of physical interest are closely related to moments of a studied distribution. $\mu_i'(g)$, the ith moment about origin of a distribution g, is defined by

$$\mu_i'(g) = \int_0^\infty x^i g(x)\,dx, \quad (10)$$

and this definition is almost identical to the definition of Mellin transformation of a function $g(x)$, which is a function of the variable t

$$\mathcal{M}\{g(x), t\} = \int_0^\infty x^{t-1} g(x)\,dx. \quad (11)$$

For example, the interesting average needle diameter, $\bar{D}$, can be expressed in terms of moments with respect to the disk diameter distribution, h_D,

$$\bar{D} = \frac{\mu_1'(h_D)}{\mu_0'(h_D)}. \quad (12)$$

With respect to the normalized disk diameter distribution $h_D^*(D) = h_D(D)/\mu_0'(h_D)$, $\bar{D}$ is simply the first moment about origin, and a common measure for the width of the diameter distribution is its variance, σ_D

$$\sigma_D = \mu_2(h_D^*) = \int_0^\infty (D - \bar{D})^2 h_D^*(D)\,dD, \quad (13)$$

the second central moment of h_D^*.

Taking Advantage of the Mellin Convolution

There is no need to invert eq. (8) before computing values for such structural parameters, which can be expressed in terms of moments $\mu_i'(h_D)$, because for any set of functions related by eq. (8) the theorem

$$\mu_i'(g_2) = \mu_i'(h_D)\mu_i'(g_c)\ \forall\ i \quad (14)$$

is valid.[8] Thus, any moment of h_D can be computed from the corresponding moment of g_2. After solving eq. (14) for $\mu_i'(h_D)$, one computes the series $\mu_i'(g_c)$ for $i = 0, 1, 2, \ldots$ from $\mathcal{M}\{g_c, t\}$, the Mellin transformed of g_c as a function of a variable t

$$\mathcal{M}\{g_c, t\} = \frac{1}{\sqrt{\pi}} \frac{\Gamma\left(\frac{t+1}{2}\right)}{\Gamma\left(\frac{t+2}{2}\right)}, \quad (15)$$

taken at $t = 1, 2, 3, \ldots$. Γ indicates the Gamma function. The moments $\mu_i'(g_2)$ of the measured chord distribution are computed by numerical integration. Central moments $\mu_i(h_D)$ can be computed from moments about origin as stated elsewhere.[8,24]

Total Needle Cross-Section per Fiber Cross-Section

If the scattering has been normalized to constant irradiated volume, and if the density contrast between particle ("needle") and matrix does not change during the experiment, the second moment about origin, $\mu_2'(h_D)$, of the disk diameter distribution

$$\mu_2'(h_D) = \int_0^\infty D^2 h_D(D)\,dD \quad (16)$$

is proportional to the total cross-section of needles per fiber cross-section, and may be studied as a function of tunable parameters.

MATERIALS AND EXPERIMENTS

The commercial poly(ether ester) (PEE) Arnitel E2000/60 (manufactured by DSM, The Netherlands) has been studied. The material is a

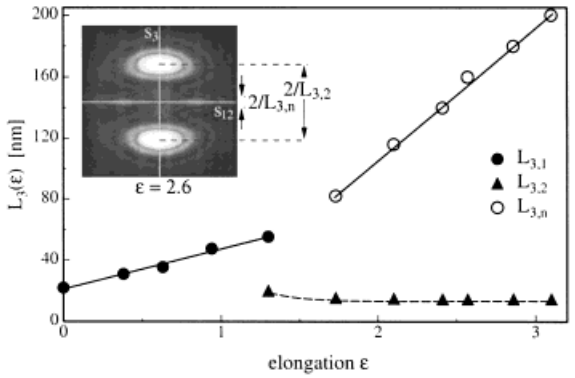

Figure 2. Principle SAXS pattern and peak shifts observed during the straining of a PEE sample. $L_{3,1}$ and $L_{3,2}$ are long periods, while $L_{3,n}$ is the reciprocal height of the form factor envelope from an ensemble of needle-shaped particles causing the equatorial scattering.

multiblock copolymer containing hard segment blocks from poly(butylene terephthalate) (PBT) and soft segment blocks from poly(tetrahydrofuran) (PTHF). As a result of phase separation a two-phase system from hard domains and soft domains is formed. With respect to material properties PEEs are thermoplastic elastomers. When strained beyond 50%, the process becomes irreversible.[25] The relation between irreversible elongation and the materials two-phase structure is supposed to be elucidated by means of a quantitative analysis of the SAXS patterns recorded during a straining experiment.

A film with a thickness of 400 μm has been strained continuously in the synchrotron beam at beamline A2 (HASYLAB, Hamburg). Image plate detector has been positioned 1.8 m behind the sample and exposed for 1 min, typically to obtain maximum accumulated count readings of approximately 60,000. The chosen semitransparent beam stop ensures a low background scattering at the expense of a relatively large blind area in the center of the pattern.

Data analysis has been carried out using published computer programs,[26] which are freely available.[27]

DATA ANALYSIS AND RESULTS

Observations and Semiquantitative Analysis

Principal observations and peak shifts are shown in Figure 2. During straining a two-point diagram (long period $L_{3,1}$) is observed. At an elongation $\epsilon = 1.3$ a second peak ($L_{3,2}$) emerges, the first peak vanishes behind the primary beam stop, and "needle scattering" ($L_{3,n}$) emerges at the equator. This observation can be explained by Peterlin's microfibrillar model.[3] At low elongation microfibrils from hard and soft domains cause the two-point pattern, while during the progress of elongation hard domains are unravelled, causing the formation of high, needle-shaped soft domains that scatter about the equator.

Projections and the Transverse Structure

According to eqs. (1) and (3) projections $\{I\}_2(s_{12})$ of the scattered intensity have been computed from all the patterns, which show the equatorial streak. The height $b(\epsilon)$ of the evaluated equatorial band as a function of the elongation ϵ was determined from the intensity minimum in s_3-direction between the equatorial streak and the off-equatorial scattering [$b(1.7) = 46$, $b(2.1) = 42$, and $b(\epsilon > 2.1) = 40$ pixels. Pixel height 1.19 10^{-3}/nm].

The projections extracted from the images in the series are presented in Figure 3. The curves show a distinct Porod region, in which the scattering falls off with s_{12}^{-3}. Small deviations are accounted to the nonideal structure of the real two-phase system and corrected according to eq. (6), leading to 2D interference functions $G_2(s_{12})$ of an ideal two-phase system.

From the interference functions the 2D chord distributions $g_2(x_{12})$ (cf. Fig. 4) have been computed following eq. (7).

In general, $g_2(x_{12})$ shows the distribution of chords from needle and matrix cross-sections, and their correlations in the plane normal to straining

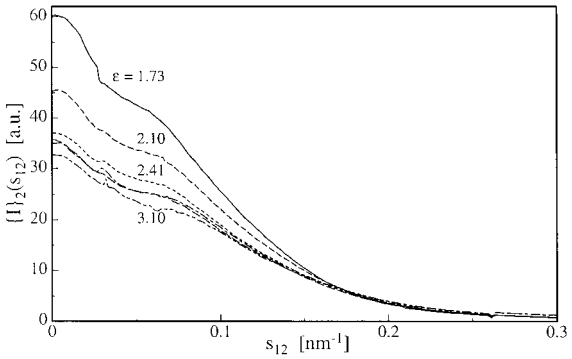

Figure 3. Projections $\{I\}_2(s_{12})$ of the equatorial scattering onto the plane normal to the straining direction as extracted from small-angle X-ray scattering patterns of a poly(ether ester) as a function of elongation ϵ.

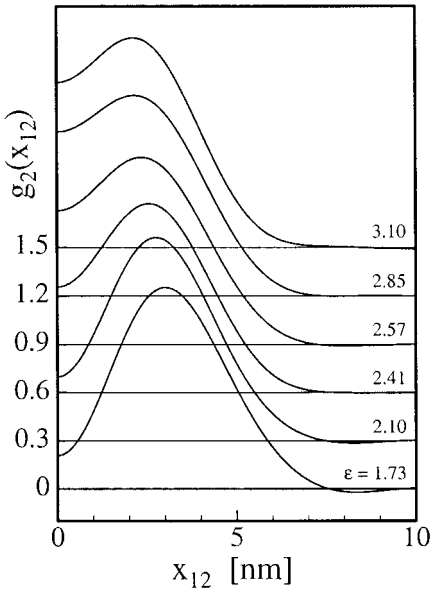

Figure 4. 2D chord distributions $g_2(x_{12})$ of a poly(ether ester) as a function of elongation ϵ, computed from the projected equatorial small-angle X-ray scattering $\{I\}_2(s_{12})$.

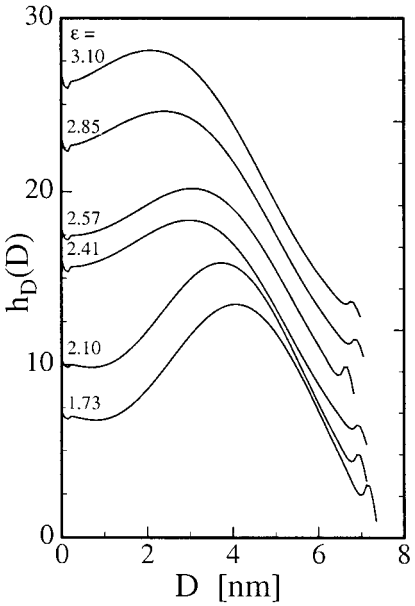

Figure 5. Soft domain needle diameter distributions, $h_D(D)$, of a poly(ether ester) as a function of elongation, ϵ, computed by numerical Mellin deconvolution from the $g_2(x_{12})$ curves shown in Figure 4. Wiggles close to the curve ends are artifacts.

direction. Experimentally, only a single positive peak from uncorrelated disks is observed, indicating that in this physical space representation the correlations among the soft domain cross-sections appear to be negligible. Thus, the simplified evaluation method deduced in the Chord Distribution Analysis section can be applied.

Figure 5 shows the diameter distributions, $h_D(D)$, of needle-shaped soft domains in a poly(ether ester) as a function of elongation, ϵ. The functions have been computed by the numerical Mellin deconvolution algorithm, which has been described in the Chord Distribution Analysis section.

Values of structural parameters, which characterize the ensemble of needle-shaped soft domains in the poly(ether ester) sample, have been determined directly from $g_2(x_{12})$, as has been deduced in the theoretical section. The results are shown in Figure 6. $\bar{D}$ (open circles) is the average needle diameter as a function of elongation, and $\sigma/\bar{D}$ (filled circles) is the relative width of the needle diameter distribution. The curve marked by squares is $\mu_2'(h_D)(\epsilon)$, the second moment about origin of the needle diameter distribution as a function of elongation ϵ. The values have been computed according to eq. (16).

DISCUSSION

From Figure 6 it is obvious that the mean diameter of the needle-shaped domains decreases almost lin-

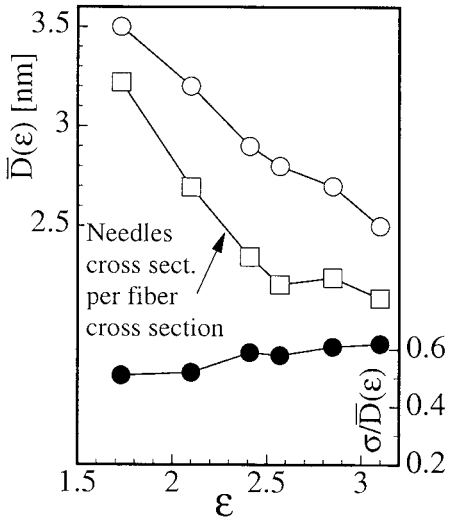

Figure 6. Characterization of the ensemble of needle-shaped soft domains in a poly(ether ester) as a function of elongation, ϵ. $\bar{D}$ (open circles) is the average needle diameter, and $\sigma/\bar{D}$ (filled circles) is the relative width of the needle diameter distribution. The curve in the middle has been computed by means of eq. (16).

early with increasing elongation, while for rubber elastic behavior, one would have expected a decrease according to $\bar{D}(\epsilon) = \bar{D}_0/\sqrt{\epsilon + 1}$. As shown in Figure 5, the reason is that the disk diameter distribution alters its shape. With increasing elongation more and more thin needles are emerging, which cause the average diameter to decrease considerably. Now, when extrapolating linearly towards $\epsilon = 0$, one finds a hypothetic average initial diameter $\bar{D}_0 = 4.8$ nm of the soft domain needles. $\sigma/\bar{D}(\epsilon)$, the relative width parameter of the disk diameter distribution, hardly increases.

The values of $\mu_2'(h_D)(\epsilon)$, which are proportional to the total needle cross-section per fiber cross-section, are constant only for elongations $\epsilon > 2.5$. On the other hand, in the observable region of elongations $1.7 < \epsilon < 2.5$ a considerable decrease is observed. This decrease indicates a strain-hardening process of the soft needles: during straining, the soft material of the needles is compressed in transverse direction with respect to the surrounding matrix material. An increase of the needle density during this process amplifies the observed effect. The measured values could be compared with measurements of Young's modulus, and stress-induced polymorphic transitions[28] could be discussed in conjunction with the presented result. To describe the shape of the disk diameter distribution more accurately by means of moments, one could proceed in the series and compute the skewness $\gamma = \mu_3(h_D)/\sigma_D^3$ of the distribution and study it as a function of elongation.[24]

In general, this work indicates that for a morphology that is both dominated by correlation and disorder, a direct analysis of the scattering pattern puts the focus on the study of long-range correlation. In an analysis of the chord distribution in physical space, on the other hand, the emphasis falls on the structures short-range disorder.

This investigation has been supported by HASYLAB Hamburg under project I-97-06. The study of the material was kindly suggested by Professor Kricheldorf, University of Hamburg. Sample material was supplied by courtesy of the DSM Corp., The Netherlands.

REFERENCES AND NOTES

1. Bonart, R. Colloid Polym Sci 1966, 211, 14.
2. Statton, W. O. Z Kristallogr 1968, 127, 229.
3. Peterlin, A. Text Res J 1972, 42, 20.
4. Rudolf, P. R.; Landes, B. G. Spectroscopy 1994, 9, 22.
5. Cohen, Y.; Thomas, E. L. J Polym Sci Part B Polym Phys 1987, 25, 1607.
6. Porod, G. Monatsh Chem 1972, 10, 395.
7. Ruland, W. J Appl Crystallogr 1970, 4, 70.
8. Stribeck, N. Colloid Polym Sci 1993, 271, 1007.
9. Méring, J.; Tchoubar–Vallat, D. C R Acad Sci Paris 1965, 261, 3096.
10. Porod, G. In Small-Angle X-Ray Scattering; Brumberger, H., Ed.; Gordon and Breach: New York, 1967, p. 1.
11. Schmidt, P. W. J Math Phys 1967, 8, 475.
12. Fronk, W.; Wilke, W. Colloid Polym Sci 1983, 261, 1010.
13. Fronk, W.; Wilke, W. Colloid Polym Sci 1985, 263, 97.
14. Wilke, W.; Lohde, U.; Pomper, T.; Karl, A.; v. Krosigk, G.; Cunis, S.; Gehrke, R. HASYLAB Annual Report, vol. I; 1977, p. 703.
15. Asherov, B. A.; Ginzburg, B. M. J Macromol Sci Phys 1997, B36, 689.
16. Murthy, N. S.; Bednarczyk, C.; Moore, R. A. F.; Grubb, D. T. J Polym Sci Part B Polym Phys 1996, 34, 821.
17. Murthy, N. S.; Zero, K.; Grubb, D. T. Polymer 1997, 38, 1021.
18. Perret, R.; Ruland, W. J Appl Crystallogr 1969, 2, 209.
19. Stribeck, N.; Reimers, C.; Ghioca, P.; Buzdugan, E. J Polym Sci Part B Polym Phys 1998, 36, 1423.
20. Tchoubar, D.; Méring, J. J Appl Crystallogr 1969, 2, 128.
21. Feigin, L. A.; Svergun, D. I. Structure Analysis by Small-Angle X-Ray and Neutron Scattering; Plenum Press: New York, 1987, p. 44.
22. Marichev, O. I. Handbook of Integral Transforms of Higher Transcendental Functions: Theory and Algorithmic Tables; Wiley: New York, 1983.
23. Glatter, O. J Appl Crystallogr 1974, 7, 147.
24. Zelen, M.; Severo, N. C. In Handbook of Mathematical Functions; Abramowitz, M.; Stegun, I. A., Eds.; Dover: New York, 1968.
25. Stribeck, N.; Sapoundjieva, D.; Denchev, Z.; Apostolov, A. A.; Zachmann, H. G.; Stamm, M.; Fakirov, S. Macromolecules 1997, 30, 1329.
26. Stribeck, N. Fibre Diffraction Rev 1997, 6, 20.
27. Link to programs: http://www.chemie.uni-hamburg.de/tmc/stribeck/.
28. Apostolov, A. A.; Boneva, D.; Baltá Calleja, F. J.; Krumova, M.; Fakirov, S. J Macromol Sci Phys 1998, 37, 543.